Title
Cortical sinus probing, S1P1-dependent entry and flow-based capture of egressing T cells.

Journal
Nature immunology, 10(1)

ISSN
1529-2908

Authors
Grigorova, Irina L
Schwab, Susan R
Phan, Tri Giang
et al.

Publication Date
2009

DOI
10.1038/ni.1682

Peer reviewed

HHS Public Access

Author manuscript

Nat Immunol. Author manuscript; available in PMC 2009 July 15.

Published in final edited form as:

Nat Immunol. 2009 January ; 10(1): 58–65. doi:10.1038/ni.1682.

Cortical sinus probing, $S1P_1$-dependent entry and flow-based capture of egressing T cells

Irina L Grigorova[1], **Susan R Schwab**[1,2,3], **Tri Giang Phan**[1,2], **Trung H M Pham**[1], **Takaharu Okada**[1,4], and **Jason G Cyster**[1]

[1]Howard Hughes Medical Institute and Department of Microbiology and Immunology, University of California San Francisco, CA 94143, USA

Abstract

The cellular dynamics of lymphocyte egress from lymph nodes are poorly defined. Here, we visualized the branched organization of lymph node cortical sinuses and found that after entry some T cells were retained while others returned to the parenchyma. Sphingosine-1-phosphate receptor 1 ($S1P_1$)-deficient T cells probed the sinus surface but failed to enter. In some sinuses T cells became rounded and moved in a unidirectional fashion. T cells traveled from cortical sinuses into macrophage-rich sinus areas. Many T cells flowed from medullary sinuses into the subcapsular space. We propose a multistep model of lymph node egress where cortical sinus probing is followed by $S1P_1$-dependent entry, capture of cells in a sinus region with flow and transport to medullary sinuses and the efferent lymph.

Naive T cells spend on average 6 to 12 hours in a lymph node before exiting into the efferent lymphatic and returning to circulation; activated T cells can be retained for longer but must also exit to reach effector sites1, 2. T cell egress depends on lymphocyte intrinsic expression of $S1P_1$ (http://www.signaling-gateway.org/molecule/query?afcsid=A000813), and the ligand, S1P, is abundant in lymph3. FTY720, a small molecule in clinical trial as an immunosuppressant, modulates $S1P_1$ function and inhibits lymphocyte egress1, 4. Traditionally, lymphocyte egress has been thought to initiate in the medullary region that is positioned facing the lymph node hilus and is flushed by lymph flowing to the efferent lymphatic2, 5, 6. However, sinuses positive for lymphatic vascular endothelial (LYVE)-1 marker are also present within the lymph node cortex, often in the part of the T zone adjacent to B cell follicles7-9. These cortical sinuses have been suggested to play a role in lymphocyte egress10-12. Previous work indicates $S1P_1$ is important for cellular localization

---

Correspondence should be addressed to Jason G. Cyster, HSE1001, Dept. Micro. & Immuno., 513 Parnassus Ave, UCSF, San Francisco, CA94143−0414; phone (415) 502−6427; Email: Jason.Cyster@ucsf.edu.

[2]These authors contributed equally to this work.

[3]Present address: Skirball Institute of Biomolecular Medicine, New York University School of Medicine, New York, New York 10016, USA.

[4]Present address: Research Center for Allergy & Immunology, RIKEN 1−7−22 Suehiro-cho Tsurumi-ku, Yokohama 230−0045

Author contributions

All authors contributed to the design of the research. I.L.G. did the majority of the experiments. S.R.S. performed several explant experiments. T.G.P. and T.O. helped establish the intravital imaging and labeling procedures and assisted in some experiments. T.H.M.P. helped with *Edg1*$^{-/-}$ fetal liver chimera preparation. I.L.G., S.R.S. and J.G.C. analyzed the data and I.L.G. and J.G.C. prepared the manuscript.

inside these cortical sinuses9. However, it has not been clear whether $S1P_1$ is needed for entry or retention, or how cells could exit the lymph node via these lymphocyte-filled structures.

An initial effort to image some aspects of T cell egress dynamics used explanted lymph nodes and observed movement of cells in and out of wheat germ agglutinin (WGA)-labeled, medullary sinus-like structures6. However, this process was not inhibited by $S1P_1$ antagonism making it unclear how it relates to the $S1P_1$-dependent egress process. A follow-up intravital study showed effects of pharmacological $S1P_1$ agonists on T cell movement in the medulla but did not examine egress dynamics13. While these studies provided some insight into the behavior of T cells in the lymph node medullary region, they have not illuminated how $S1P_1$ functions within the T cell during egress.

Here we have used antibodies to LYVE-1 to intravitally label sinuses in the cortical region9 as well as sinuses and macrophages14 in the medullary region. We show that $S1P_1$-deficient T cells migrated over and probed the surface of cortical sinuses in a similar manner to wild-type T cells, but they were inefficient at entering these structures. Wild-type T cells entered and exited cortical sinuses. While cortical sinus side branches showed little evidence of flow, T cells were often observed to flow unidirectionally in central branches. Such flow carried T cells to macrophage-rich sinus structures in medullary or interfollicular regions. Imaging of medullary regions showed T cell ‘release’ from sinuses into the subcapsular lymph for exit from the lymph node. These observations allow us to propose a multi-step model of lymph node egress.

Results

Distribution of LYVE-1$^+$ sinuses

Our initial goal in this study was to examine the cellular dynamics of the earliest $S1P_1$-dependent step in lymph node egress and we therefore focused on cortical sinuses as candidate sites of egress commitment. By immunohistochemical analysis, LYVE-1$^+$ cortical sinuses were identified in T cell areas proximal to B cell follicles, and often these sinuses appeared to connect between two separated macrophage-rich interfollicular areas (Fig. 1a and Supplementary Fig. 1 online). In other cases LYVE-1+ cortical sinuses could be observed connecting to the macrophage-rich medulla (Fig. 1b). Consistent with other studies14, LYVE-1 staining in interfollicular and medullary areas was not restricted to the lymphatic cells lining sinuses but also included many associated CD169$^+$ macrophages (Fig. 1b). To facilitate imaging of cortical sinuses within inguinal lymph nodes (Fig. 1c) we used a modified intravital preparation where a small window was introduced in the skin above the inguinal lymph node in the surgically exposed skin flap15. Mice were injected subcutaneously with fluorescently labeled LYVE-1-specific antibody one day prior to image analysis, and T cells labeled with a red dye were also injected. As shown in a three-dimensional projection view (Fig. 1d and Supplementary Movie 1 online) this approach allowed us to visualize LYVE-1$^+$ cortical sinuses in the intact lymph node in areas free of macrophages and surrounded by T cells. These structures often showed a complex branching morphology that included side branches as well as central branches that connected to macrophage-rich sinus regions (Fig. 1c, d and Supplementary Movie 1).

Sinus probing and entry

Image analysis of T cell behavior in the proximity of LYVE-1 labeled cortical sinuses showed that both wild-type cells and $S1P_1$-deficient cells (lacking the $S1P_1$ encoding *Edg1* gene) approach and migrate over the sinus surface (Fig. 2a–b, and Supplementary Movie 2 online). However, compared to wild-type T cells, $S1P_1$-deficient T cells were severely compromised in their ability to enter cortical sinuses (Fig. 2b–c, see also schematic in Supplementary Fig. 2a online). Similar findings were made in intravital and in explant experiments (Fig. 2c). When averaged across four experiments, approximately 25% of wild-type cells that contacted LYVE-1^+ cortical sinuses entered into the lumen whereas the entry of $S1P_1$-deficient cells was markedly less efficient with only about 2% of encounters resulting in entry (Fig. 2c, top). The LYVE-1^+ cortical sinus structures are thin-walled and in a small number of cases clear discrimination of whether a cell was at the border or inside the sinus was not possible. We therefore also represent the data with an overestimating assumption that all indistinguishable cells did migrate inside the structures (Fig. 2c, bottom). Even with this scoring, the $S1P_1$-deficient cells showed an entry efficiency that was less than 20% of the entry efficiency observed for wild-type cells. By contrast, the behavior of wild-type and $S1P_1$-deficient T cells at the sinus border was very similar. Both cell types showed a tendency to migrate along the LYVE-1^+ sinus surface following encounter, with some cells remaining associated for more than 10 min (Fig. 2d and Supplementary Movie 2). $S1P_1$-deficient cells were associated with the border for slightly longer than wild-type cells, perhaps secondary to their inability to enter into the sinuses (Fig. 2d). The median velocities of wild-type and $S1P_1$-deficient cells in the T zone adjacent to cortical sinuses and at the sinus outer border were similar (Fig. 2e). $S1P_1$-deficient and wild-type T cells showed a similar propensity to move in the direction of the sinuses, suggesting that $S1P_1$ is not critical for naive T cell migration toward the sinuses (Fig. 2f). Wild-type T cells appeared to enter cortical sinuses at multiple locations (Supplementary Movie 2). However, in agreement with an analysis of cell entry to medullary WGA^+ sinuses6, we sometimes observed instances of two or more labeled cells entering at an overlapping location, a possible entry ‘hot-spot’ (Supplementary Movie 2).

Since we observed a similar $S1P_1$ requirement for cortical sinus entry in intravital and explant preparations, we took advantage of the superior stability of the explant system to obtain high resolution imaging data that occasionally allowed cell processes to be resolved. Wild-type cells could be observed encountering LYVE-1^+ structures and extending a process through the wall into the sinus lumen (Fig. 3a and Supplementary Movie 3 online). Moments later these cells would either retract the process and move away or transmigrate into the sinus lumen (Fig. 3b and Supplementary Movie 3). $S1P_1$-deficient cells could also be seen extending processes into the sinus lumen before retracting, re-orientating and moving away (Fig. 3c,d and Supplementary Movie 3). These observations suggest that the cellular ‘decision-making’ during sinus entry occurs when cells probe the sinus wall.

Directional flow of T cells in central sinusoids

We next asked whether we could detect directional cell movement within cortical sinuses. In the course of multiple imaging experiments we observed stable lymph flow through the subcapsular sinus in the first ∼2 h after anesthesia and surgery, and this was confirmed by

the efficient drainage of subcutaneously injected phycoerythrin (PE) into medullary sinuses (Supplementary Movie 4 online). However, at later times the flow was reduced, in agreement with the requirement for active muscular activity to maintain maximal peripheral lymph flow16, 17. We therefore focused our imaging experiments testing for cortical sinus flow during the first 2 h after anesthesia and surgery. To facilitate tracking of cells within cortical sinuses we used Imaris software (see Methods) to generate a reconstruction of the sinus structures, distinguishing the cortical sinuses from macrophage-rich sinuses near the capsule (Fig. 4a and Supplementary Movie 5 online). Reconstructions were generated by tracing the outline of the sinus in each individual *z*-plane at several time points (Supplementary Fig. 2b-d online). By examining cell behavior within the lumen of several cortical sinus branches it was evident that in some, usually larger, branches the majority of T cells moved in the same direction with almost uniform intralumenal paths (Fig. 4a and Supplementary Movie 5 **online**). When the tracks for a given branch were plotted on *x*–*y* plots the unidirectional flux of T cells in these branches was striking (Fig. 4b, branches IV and V in Fig. 4a) as opposed to the adjacent branches that exhibited essentially random T cell migration (Fig. 4b, branches I and II in Fig. 4a). Rare cells were detected that moved along the wall of the sinus in a direction against the flow (Fig. 4b, brown track in the last panel). Comparison of cell morphologies suggested the cells in a sinus region with flow were more rounded than cells in other regions (Fig. 4c,d). Measurement of the longest and shortest cell dimensions showed that cells in a region of flow had an axis ratio close to one, consistent with a rounded morphology whereas cells in other regions often had an elongated morphology with a length that was two or three-fold greater than their width (Fig. 4c,d). It is notable that T cells in a region of flow shared rather uniform velocities (Fig. 4e). Although moving unidirectionally and apparently flowing rather than actively migrating, T cells in a region of flow showed slower overall velocities than cells in the T zone or in sinus regions without flow (Fig. 4e,f). Interestingly, cell velocities in the parenchyma and inside the sinuses without flow were not significantly different (Fig. 4e,f). Cells migrated for variable and often short amounts of time inside the cortical sinus areas without evidence of flow, and about 50% of the cells migrated back into the T zone within 30 min (Fig. 4g,h). By contrast, T cells in a sinus showing evidence of flow were strongly retained and very few cells left through the walls of the structure into the T zone (Fig. 4g,h). Occasionally cells that transited from a region of active migration to a region of flow were detected (Fig. 4i and Supplementary Fig. 3 online). Upon making this transition the cells underwent a reduction in velocity and became more rounded (Fig. 4j,k). Some T cells could also be seen migrating from the parenchyma into cortical sinuses in a region with flow and becoming captured in the flow (data not shown).

Release of T cells in macrophage-rich sinuses

Connections between cortical and medullary sinuses were often deep in the tissue and difficult to image but occasionally these were resolved (Supplementary Movie 6 online). Wild-type T cells could be seen flowing in the sinuses whereas both wild-type and $S1P_1$-deficient T cells were present in the T zone and $S1P_1$-deficient T cells were observable in LYVE-1^- medullary areas (Supplementary Movie 6). In the medulla it was sometimes difficult to resolve the sinus and non-sinus areas amongst the macrophages. This is likely because of the co-expression of LYVE-1 by some of the lymphatic-associated macrophages

(Fig. 1b) and because the elastic capsule of the lymph node and the reduced lymph flow under anesthesia may cause a reduction in sinus diameters and flow rates. In some cases, upon reaching a macrophage-rich sinus region, the sinusoidal T cells became poorly mobile, perhaps adherent to the macrophages (Fig. 5a, Supplmentary Fig. 3c and Supplementary Movies 6,7 online). Occasionally these T cells resumed migration and returned to the T zone (Supplementary Fig. 3c). In agreement with recent work6, 13, 18, wild-type T cells in the medullary regions had reduced migration velocities (Fig. 5b and Supplementary Movies 6,7) compared to their velocities in the parenchyma (Fig. 2e). When the medulla was divided into LYVE-1^+ and LYVE-1^- regions and the border between them, it was evident that LYVE-1^+ regions were enriched for wild-type T cells and LYVE-1^- regions for $S1P_1$-deficient T cells (Fig. 5a,c and Supplementary Movies 6,7). $S1P_1$-deficient T cells showed on average greater velocities than wild-type T cells in the medulla (Fig. 5a,b), however, it is notable that the same trend for slower T cell movement within LYVE-1^+ regions was observed for both cell types (Fig. 5a,c and Supplementary Movie 7). When the surface of the medulla was imaged from the hilar side of the lymph node, the openings of medullary sinuses into subcapsular regions near the efferent vessel were sometimes visible, and T cells were observed being released into the subcapsular region and moving off rapidly with the lymph flow (Fig. 5d and Supplementary Movies 8,9 online). Thus, T cell passage through medullary sinus regions is multi-faceted, with some cells becoming migratory and returning to the parenchyma and others flowing rapidly through sinuses that open into the lymph node hilus.

Discussion

Formulation of the multi-step paradigm of cell entry from blood into tissues depended on findings from a large series of molecular perturbation and real-time imaging studies (reviewed in 2, 19, 20). Here we used similar approaches to begin illuminating the complex and distinct dynamics of S1P-dependent T cell egress from lymph nodes. Our findings support a multi-step model of T cell egress from lymph nodes where cortical sinus probing and $S1P_1$-mediated entry are followed by capture in a region of flow, passage to medullary sinuses and subsequent flushing into the subcapsular space and efferent lymph (Supplementary Fig. 4 online). We suggest that the critical cellular decision-making during egress occurs as the T cell probes the cortical sinus surface and receives an amplifying Gαi-signal via $S1P_1$ that allows the sinus-associated cellular process to ‘win-out’ and become the leading edge of the cell.

The existence of flow within cortical sinuses was unexpected though a small number of lymph tracer studies have favored this possibility21, 22. The ‘looping’ three-dimensional organization of cortical sinuses is consistent with lymph entering from subcapsular or medullary sinuses and then traveling through cortical sinus branches that reconnect to medullary or interfollicular sinuses. We speculate that macrophage-filtered fluid reaches cortical sinuses to varying extents depending on the amount and flow rate of incoming lymph. Anaesthesia causes a 50% decrease in thoracic duct lymph flow in rats16 and flow in peripheral lymphatics can be reduced as much as 80% (ref. 17). Studies in sheep and humans have shown that sleep or physical rest reduces the flow of lymph in cannulated efferent vessels and there is an associated decrease in lymphocyte output in the efferent

lymph23, 24. The multi-step model of T cell egress we outline here suggests that in addition to dependence on $S1P_1$, egress dynamics will be sensitive to lymph flow rates.

Our observation that exit 'decision-making' appears to occur at the cortical sinus surface supports a 'competing cues' model, where T cells encountering sinusoids would have a choice of responding to S1P and entering the sinus or continuing to respond to the chemokine CCL21 (or other T zone attractants) and moving back into the T zone9. In this model, the amount and sensitivity of each receptor expressed by the cell and the amount of ligand encountered, rather than a unique signaling input, would determine the cellular behavior that 'wins-out'. The finding that even two-fold changes in the amount of $S1P_1$ or CCR7 (http://www.signaling-gateway.org/molecule/query?afcsid=A000630) on the T cell can markedly alter egress efficiency is consistent with this model9. The propensity of wild-type cells to readily exit from cortical sinusoids lacking flow may be because the cells encounter CCL21 as they probe the outer surface of the structure. $S1P_1$ is sensitive to rapid desensitization by ligand25 whereas CCR7 is quite resistant to ligand-induced desensitization26; modulation of $S1P_1$ expressed on lumenal T cells may facilitate dominance by CCL21 and return to the T zone. However, the ability of T cells to migrate within sinus structures without flow raises a question of chemokines or other factors that promote motility inside the lumen, and a possible role for S1P in this process is not excluded. Moreover, since so few $S1P_1$-deficient cells entered cortical sinuses, it was not possible for us to determine whether $S1P_1$ contributes to T cell retention within these structures. Finally, although we did not detect a role for $S1P_1$ in promoting directional migration of naive T cells toward cortical sinuses, it remains possible that under conditions where T zone chemokine or chemokine receptor expression are reduced9, 27, the action of an S1P gradient will become evident.

The extent to which T cells egress lymph nodes through entry into cortical sinuses versus direct migration into medullary sinuses is not thoroughly addressed in this study, though the low number of wild-type cells outside of LYVE-1 positive structures in the medullary region compared to the high T cell density around cortical sinuses is consistent with cortical sinuses acting as a major egress pathway. Although T cell densities in the medulla are low, the presence of greater numbers of $S1P_1$-deficient than wild-type T cells in medullary areas adjacent to LYVE-1^+ structures suggests that the principles we have observed for T cell entry to cortical sinuses may apply to medullary sinuses. We also observed rare T cells moving from interfollicular regions into the subcapsular sinus (I.L.G. & J.G.C., unpubl. obs.) suggesting that some egress may occur at these sites.

Previous work demonstrated that treatment with SEW2871, an $S1P_1$ agonist, led to a block in T cell motility in the medullary region and subsequent exposure to an $S1P_1$ antagonist could restore motility, including an ability to enter WGA^+ sinus-like structures6, 13. Exposure to the $S1P_1$ antagonist alone appeared to have no effect. We consider it likely that the inability of the antagonist to block entry into medullary sinuses is a consequence of the low potency of the antagonist28 compared to the potency of S1P in promoting egress and the abundance of this lipid in lymph3. Moreover, the analysis of sinus-like structures in the published work was in an explant setting, and thus in the absence of physiological flow. Consistent with the previous studies, we observed that T cell motility was lower in

LYVE-1$^+$ medullary regions. Wild-type T cells in this region often seemed almost immobile, perhaps reflecting adhesive interactions between T cells and macrophages. Macrophages have previously been implicated in lymphoid tissue 'trapping' of T cells29 and T cells inside macrophage-rich granulomas show a reduction in migration velocities compared to cells in surrounding tissue30. T cells can bind macrophages via numerous surface molecules including sialoadhesin (CD169)31, 32. S1P$_1$-deficient cells appeared on average to have higher motility in the medulla, a finding that at face value seems consistent with the reduced motility of wild-type cells following exposure to the agonist SEW2871 (refs. 6, 13). However, in the previous work it was proposed that the agonist reduced motility by acting on stromal cells to close medullary egress portals and cause 'log-jamming' of T cells. Such an explanation cannot be applied to our observations since we examine the contribution of S1P$_1$ in the T cell, not in the stromal cell. We favor the interpretation that the different velocities of S1P$_1$-deficient and wild-type medullary T cells is because 'knockout' T cells are mostly migrating within macrophage-sparse medullary regions, whereas many wild-type cells are within sinuses attached to sinus-associated macrophages.

Whether lymphocytes cross the LYVE-1$^+$ cell layer at endothelial junctions or between cells is not yet clear. In previous work an example of several cells entering and exiting a WGA$^+$ medullary sinus-like structure at a common location led to the proposal that medullary sinuses contain egress portals6. In our experiments we observed cells entering and exiting a single LYVE-1$^+$ cortical sinus at multiple locations. There were also examples of cells that appeared to follow one another through a single location consistent with the existence of 'portals' or preferred transmigration spots. Ultrastructural studies of cortical sinuses have disagreed on whether preformed pores do10, 33 or do not exist21, 34. The ability of the tracer molecules ferrypolymaltose, ferritin and horseradish peroxidase to gain access to sinuses but not the surrounding parenchyma21, 22 favors the view that the 'openings' only occur as cells cross. The junctions between lymphatic endothelial cells are distinct from the tight junctions that form between typical blood vessel endothelial cells and in some cases involve 'buttonlike' contacts and flaps that may act as cell entry sites35. Higher resolution dynamic analysis will be required to determine the extent to which cells enter cortical sinuses via 'hotspots' and to better define the properties of the LYVE-1$^+$ cells at these sites.

Methods

Mice

6−12 week old wild-type Ly5.1 (CD45.2) and Ly5.2 (CD45.1) congenic C57BL/6 mice were purchased from either the National Cancer Institute or Jackson Laboratories or were from a colony maintained at the University of California, San Francisco. C57BL/6 mice expressing GFP (004353; Tg(UBCGFP)30Scha/J) or CFP (004218; Tg(ACTB-ECFP)) and mice deficient for *Rag1* (002216: *Rag1*^{tm1Mom}) were from Jackson Laboratories. *Edg1*$^{+/-}$ mice were provided by R. Proia (NCI). S1P$_1$-deficient thymocytes and control S1P$_1$-positive thymocytes were generated by reconstitution of irradiated Ly5.2 or *Rag1*$^{-/-}$ mice with E12.5 fetal liver cells of *Edg1*$^{-/-}$ and *Edg1*$^{+/+}$ littermates as described36 or with bone marrow from *Edg1*$^{-/-}$ and *Edg1*$^{+/+}$ fetal liver chimeras. Animals were housed in a specific-pathogen free

environment in the Laboratory Animal Research Center at UCSF, and all experiments conformed to ethical principles and guidelines approved by the UCSF Institutional Animal Care and Use Committee.

Cell isolation, labeling, adoptive transfers and flow cytometry

$S1P_1$-deficient and wild-type thymocytes were isolated by mechanical disruption on 70-μm nylon cell strainers (Falcon) in RPMI medium (Cellgro) containing 1% fetal bovine serum (FBS, HyClone), antibiotics (50 IU/ml of penicillin and 50 μg/ml of streptomycin; Cellgro) and 10 mM HEPES pH7.2 (Cellgro), and then were washed. T cells from UBC-GFP mice and B cells from CFP^+ mice were isolated from spleen and peripheral and mesenteric lymph nodes as described37 using the AutoMACS cell separator (Miltenyi Biotech) and biotinylated mAbs to CD11b (clone M1/70.15, CALTAG Laboratories), CD11c (clone HL3, BD Pharmingen), CD45R/B220 (clone RA3−6B2, BD Pharmingen or CALTAG Laboratories), and Gr-1 (clone RB6−8C5, BD Pharmingen) (for T cell purification) and CD11c and CD43 clone S7 (from BD Biosciences) (for B cell purification) and MACS streptavidinmicrobeads (Miltenyi Biotech). B cell and T cell purities were typically greater than 95% pure. Thymocytes or T cells were labeled either with 10 μM of carboxyfluorescein diacetate succinimidyl ester (CFSE; Invitrogen/Molecular Probes) or with 20 μM of 5-(and-6)-(((4-chloromethyl)benzoyl)amino)-tetramethylrhodamine (CMTMR; Invitrogen/Molecular Probes) or double labeled with CFSE and CMTMR simultaneously in DMEM or RPMI containing 1% FBS for 20 min at 37 °C then washed by spinning through a layer of FBS. Labeled cells were adoptively transferred into the lateral tail vein by intravenous injection. Lymphocyte preparations before adoptive transfer and lymph node cells post-imaging were stained with various fluorochrome-conjugated antibodies from BD Pharmingen as described38, and data were acquired on an FACS Calibur (BD) and analyzed with FlowJo software (Treestar).

Confocal microscopy

Inguinal lymph nodes were isolated either from intact C57BL/6 mice or from C57BL/6 mice 12 h after injection s.c. in the flanks and tail base with 30 μg of rat mAbs to LYVE-1 clone 223322 (R & D Systems) conjugated to Texas Red and injected i.v. with $\sim 10^7$ GFP^+ T cells. Some of the nodes were then fixed in 4% paraformaldehyde solution in PBS for 12 h and then incubated in 18% sucrose solution in PBS for 24 h. 10−30 μm cryostat sections were blocked with 4% normal rat serum and 4% normal mouse serum and stained with MOMA-1 mAb conjugated to Alexa Fluor 647 and anti-LYVE-1 mAb conjugated to Texas Red. Alternatively, sections were blocked with 4% normal mouse serum and stained with MOMA-1 hybridoma supernatant detected with anti-rat IgG (H+L) $F(ab)_2$ fluorescein isothiocyanate (FITC) (Jackson Immunosearch). Sections were then blocked with 4% normal rat serum before incubation with anti-LYVE-1-biotin and streptavidin-Alexa Fluor 647. Images were acquired on a Leica TCS SP2 confocal microscope (Leica Microsystems) using the 488, 594 and 633 nm laser lines to excite Alexa Fluor 488, Texas Red and Alexa Fluor 647, respectively. Emission slits were tuned to 498−550 nm for Alexa Fluor 488, 604−625 nm for Texas Red and 650−700 nm for Alexa Fluor 647. Confocal images were processed using MetaMorph software (Molecular Devices) and Adobe PhotoShop CS2.

Intravital microscopy and two-photon imaging

Explanted lymph nodes were prepared for imaging essentially as described39. Images were acquired with Video Savant (IO Industries) and maximum intensity time-lapse images generated with MetaMorph (Molecular Devices). Cell shape analysis, cell tracks, 3-D rotation images and LYVE-1^+ structure reconstructions were made with Imaris 5.01 × 64 (Bitplane). Calculations of the T cell entry frequencies, the time periods spent at the outer border or inside LYVE-1^+ sinuses, the median velocities of cells, as well as reconstruction of cell trajectories from the same starting point were performed using software programmed in MatLab (MathWorks). See Supplementary Methods online for additional details.

Statistical analysis

All statistical analysis was performed in GraphPad Prism (GraphPad Software). For comparison of multiple non-parametric data sets we used the Kruskal-Wallis test followed by Dunn's post-test comparison between multiple groups. For comparison of two non-parametric data sets we used the Mann-Whitney U-test. The means between two groups were compared using a one-tailed students' t test.

Supplementary Material

Refer to Web version on PubMed Central for supplementary material.

Acknowledgements

We thank A. Bullen and M. Krummel for help with the 2-photon microscope, R. Proia for $S1P_1$-deficient mice, L. Shiow for help with movie preparation and J. An for colony management. I.L.G. is a Cancer Research Institute Fellow, S.R.S. was supported by the Irvington Institute for Immunological Research, T.G.P. is supported by the National Health & Medical Research Council and American Australian Association, T.H.M.P. was supported by the Boyer Graduate Program in the Biochemical Sciences and J.G.C. is an Investigator of the Howard Hughes Medical Institute. This work was supported in part by grants from the National Institutes of Health.

References

1. Schwab SR, Cyster JG. Finding a way out: lymphocyte egress from lymphoid organs. Nat. Immunol. 2007; 8:1295–1301. [PubMed: 18026082]
2. von Andrian UH, Mempel TR. Homing and cellular traffic in lymph nodes. Nat. Rev. Immunol. 2003; 3:867–878. [PubMed: 14668803]
3. Pappu R, et al. Promotion of Lymphocyte Egress into Blood and Lymph by Distinct Sources of Sphingosine-1-Phosphate. Science. 2007; 316:295–298. [PubMed: 17363629]
4. Rosen H, Goetzl EJ. Sphingosine 1-phosphate and its receptors: an autocrine and paracrine network. Nat. Rev. Immunol. 2005; 5:560–570. [PubMed: 15999095]
5. Picker, LJ.; Siegelman, MH. Lymphoid tissues and organs. In: Paul, WE., editor. Fundamental Immunology. Vol. 4. Lippincott-Raven; Philadelphia: 1999. p. 479-531.
6. Wei SH, et al. Sphingosine 1-phosphate type 1 receptor agonism inhibits transendothelial migration of medullary T cells to lymphatic sinuses. Nat. Immunol. 2005; 6:1228–1235. [PubMed: 16273098]
7. Prevo R, Banerji S, Ni J, Jackson DG. Rapid plasma membrane-endosomal trafficking of the lymph node sinus and high endothelial venule scavenger receptor/homing receptor stabilin-1 (FEEL-1/CLEVER-1). J. Biol. Chem. 2004; 279:52580–52592. [PubMed: 15345716]
8. Hirakawa S, et al. VEGF-A induces tumor and sentinel lymph node lymphangiogenesis and promotes lymphatic metastasis. J. Exp. Med. 2005; 201:1089–1099. [PubMed: 15809353]

9. Pham TH, Okada T, Matloubian M, Lo CG, Cyster JG. S1P1 receptor signaling overrides retention mediated by G alpha i-coupled receptors to promote T cell egress. Immunity. 2008; 28:122–133. [PubMed: 18164221]
10. Belisle C, Sainte-Marie G. Tridimensional study of the deep cortex of the rat lymph node. III. Morphology of the deep cortex units. Anat. Rec. 1981; 199:213–226. [PubMed: 7212321]
11. Kelly RH. Functional anatomy of lymph nodes. I. The paracortical cords. Int. Arch. Allergy Appl. Immunol. 1975; 48:836–849. [PubMed: 49306]
12. He Y. Scanning electron microscope studies of the rat mesenteric lymph node with special reference to high-endothelial venules and hitherto unknown lymphatic labyrinth. Arch. Histol. Jpn. 1985; 48:1–15. [PubMed: 4015330]
13. Sanna MG, et al. Enhancement of capillary leakage and restoration of lymphocyte egress by a chiral S1P(1) antagonist in vivo. Nat. Chem. Biol. 2006; 2:434–441. [PubMed: 16829954]
14. Martens JH, et al. Differential expression of a gene signature for scavenger/lectin receptors by endothelial cells and macrophages in human lymph node sinuses, the primary sites of regional metastasis. J. Pathol. 2006; 208:574–589. [PubMed: 16440291]
15. Phan TG, Grigorova I, Okada T, Cyster JG. Subcapsular encounter and complement-dependent transport of immune complexes by lymph node B cells. Nat. Immunol. 2007; 8:992–1000. [PubMed: 17660822]
16. Yamada S, Kubo M, Hayashida Y. Lymph flow dynamics into the thoracic duct of the rat. Jpn. J. Physiol. 1988; 38:729–733. [PubMed: 3221524]
17. Dahan A, Mendelman A, Amsili S, Ezov N, Hoffman A. The effect of general anesthesia on the intestinal lymphatic transport of lipophilic drugs: comparison between anesthetized and freely moving conscious rat models. Eur. J. Pharm. Sci. 2007; 32:367–374. [PubMed: 17980560]
18. Nombela-Arrieta C, et al. A central role for DOCK2 during interstitial lymphocyte motility and sphingosine-1-phosphate-mediated egress. J. Exp. Med. 2007; 204:497–510. [PubMed: 17325199]
19. Kunkel EJ, Butcher EC. Chemokines and the tissue-specific migration of lymphocytes. Immunity. 2002; 16:1–4. [PubMed: 11825560]
20. Ley K, Laudanna C, Cybulsky MI, Nourshargh S. Getting to the site of inflammation: the leukocyte adhesion cascade updated. Nat. Rev. Immunol. 2007; 7:678–689. [PubMed: 17717539]
21. Nicander L, Nafstad P, Landsverk T, Engebretsen RH. A study of modified lymphatics in the deep cortex of ruminant lymph nodes. J. Anat. 1991; 178:203–212. [PubMed: 1810927]
22. Compton CC, Raviola E. Structure of the sinus-lining cells in the popliteal lymph node of the rabbit. Anat. Rec. 1985; 212:408–423. [PubMed: 4073555]
23. Dickstein JB, Hay JB, Lue FA, Moldofsky H. The relationship of lymphocytes in blood and in lymph to sleep/wake states in sheep. Sleep. 2000; 23:185–190. [PubMed: 10737335]
24. Engeset A, Sokolowski J, Olszewski WL. Variation in output of leukocytes and erythrocytes in human peripheral lymph during rest and activity. Lymphology. 1977; 10:198–203. [PubMed: 609275]
25. Schwab SR, et al. Lymphocyte sequestration through S1P lyase inhibition and disruption of S1P gradients. Science. 2005; 309:1735–1739. [PubMed: 16151014]
26. Stachowiak AN, Wang Y, Huang YC, Irvine DJ. Homeostatic lymphoid chemokines synergize with adhesion ligands to trigger T and B lymphocyte chemokinesis. J. Immunol. 2006; 177:2340–2348. [PubMed: 16887995]
27. Mueller SN, et al. Regulation of homeostatic chemokine expression and cell trafficking during immune responses. Science. 2007; 317:670–674. [PubMed: 17673664]
28. Davis MD, Clemens JJ, Macdonald TL, Lynch KR. Sphingosine 1-phosphate analogs as receptor antagonists. J. Biol. Chem. 2005; 280:9833–9841. [PubMed: 15590668]
29. Frost P. Further evidence for the role of macrophages in the initiation of lymphocyte trapping. Immunology. 1974; 27:609–616. [PubMed: 4140147]
30. Egen JG, et al. Macrophage and T cell dynamics during the development and disintegration of mycobacterial granulomas. Immunity. 2008; 28:271–284. [PubMed: 18261937]
31. van den Berg TK, et al. Sialoadhesin on macrophages: its identification as a lymphocyte adhesion molecule. J. Exp. Med. 1992; 176:647–655. [PubMed: 1512534]

32. Suzuki K, Kumanogoh A, Kikutani H. Semaphorins and their receptors in immune cell interactions. Nat. Immunol. 2008; 9:17–23. [PubMed: 18087252]

33. Crivellato E, Mallardi F. The sinus endothelial cell architecture in the mouse lymph node. Structural peculiarities and close correlation with the fibroblastic reticular cells. J. Submicrosc. Cytol. Pathol. 1998; 30:495–502. [PubMed: 9851057]

34. Heath TJ, Spalding HJ. Pathways of lymph flow to and from the medulla of lymph nodes in sheep. J. Anat. 1987; 155:177–188. [PubMed: 3503048]

35. Baluk P, et al. Functionally specialized junctions between endothelial cells of lymphatic vessels. J. Exp. Med. 2007; 204:2349–2362. [PubMed: 17846148]

36. Matloubian M, et al. Lymphocyte egress from thymus and peripheral lymphoid organs is dependent on S1P receptor 1. Nature. 2004; 427:355–360. [PubMed: 14737169]

37. Allen CD, Okada T, Tang HL, Cyster JG. Imaging of germinal center selection events during affinity maturation. Science. 2007; 315:528–531. [PubMed: 17185562]

38. Lo CG, Xu Y, Proia RL, Cyster JG. Cyclical modulation of sphingosine-1-phosphate receptor 1 surface expression during lymphocyte recirculation and relationship to lymphoid organ transit. J. Exp. Med. 2005; 201:291–301. [PubMed: 15657295]

39. Okada T, et al. Antigen-engaged B cells undergo chemotaxis toward the T zone and form motile conjugates with helper T cells. PLoS Biol. 2005; 3:e150. [PubMed: 15857154]

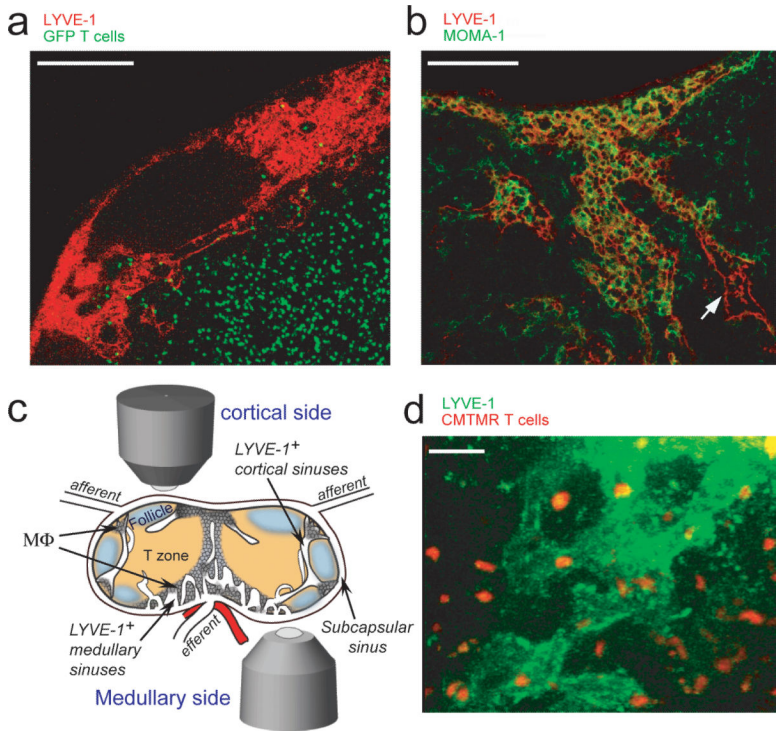

Figure 1. Morphology and distribution of LYVE-1$^+$ cortical sinuses

(a) Projection of confocal images spanning a 6 μm thick section of inguinal lymph node with transferred GFP$^+$ T cells (green) stained with LYVE-1 specific antibody (red). Scale bar, 200 μm. **(b)** Confocal microscopy of a lymph node section stained with LYVE-1 specific antibody (red) and with MOMA-1 specific antibody (green) to detect sinus-lining macrophages. A macrophage free cortical sinus (arrow) connects to LYVE-1$^+$ sinuses near the medulla that are filled with MOMA-1$^+$ macrophages, some of which are also LYVE-1$^+$. Scale bar, 100 μm. **(c)** Schematic of connections between subcapsular, cortical and medullary LYVE-1$^+$ sinuses in an inguinal lymph node. The major structures and regions are labeled. Gray circle shading indicates macrophage-rich areas. Positions of the objectives indicate cortical and medullary areas of inguinal lymph node subjected to two-photon intravital microscopy. **(d)** Projection view of a LYVE-1$^+$ cortical sinus structure in an explanted inguinal lymph node observed using two-photon microscopy. Shown as a projection view of a 214 μm z-stack. LYVE-1$^+$ sinuses are labeled with LYVE-1 specific antibody (green) and T cells with CMTMR (red). Scale bar, 30 μm. See also Supplementary Movie 1. Data in a, b and d are representative of inguinal lymph nodes from at least 3 mice.

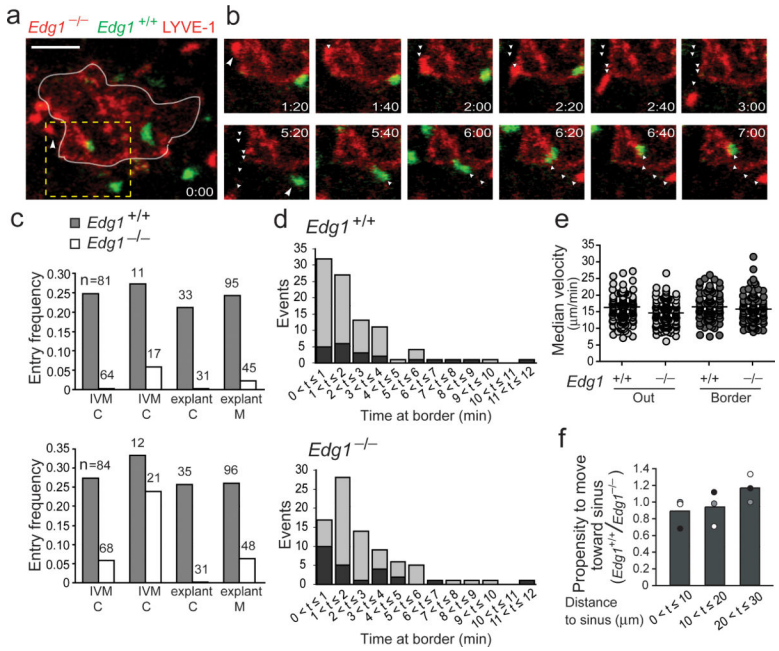

Figure 2. T cell entry into LYVE-1$^+$ cortical sinuses is dependent on S1P$_1$

(a-b) Two-photon intravital imaging of inguinal lymph node at its cortical side. *Edg1*$^{+/+}$ (GFP$^+$, green) and *Edg1*$^{-/-}$ (labeled with CMTMR, red) T cells were transferred 12 hours prior to imaging. LYVE-1$^+$ sinuses are also labeled red. 21 μm z projection. Elapsed time is shown as mm:ss. **(a)** Shows a video frame containing a LYVE-1$^+$ cortical sinus. White line follows contours of the LYVE-1$^+$ sinus wall. Dotted yellow square indicates the area presented in the time lapse images in b. Arrow points to the *Edg1*$^{-/-}$ T cell followed in the top panels of b. Scale bar, 30 μm. **(b)** Corresponding time-lapse images of *Edg1*$^{-/-}$ (red, top panel) and *Edg1*$^{+/+}$ (green, bottom panel) T cells in relation to a sub-region of the LYVE-1$^+$ cortical sinus. The path of an *Edg1*$^{-/-}$ cell is tracked (arrow heads) from 1:20 to 5:20 min and then the path of an *Edg1*$^{+/+}$ cell is tracked from 5:20 to 7:00 min. See also Supplementary Movie 2. **(c)** Frequency of entry to LYVE-1$^+$ sinuses for *Edg1*$^{+/+}$ and *Edg1*$^{-/-}$ T cells. Three-dimensional reconstruction of fluorescently labeled LYVE-1$^+$ structures was performed as described in Methods. T cell positions relative to the outside, inside and border of the cortical sinuses were assessed in every *z* plane of the image. Entry frequency is the ratio of entry events for cells starting at the outer sinus border versus the total events leaving the outer border. In a small number of cases clear discrimination of whether a cell was at the border of the sinus or transmigrated inside was not possible. Therefore, calculation of the entry frequency was performed both excluding these cases (top panel) or using a frequency-overestimating assumption that all of the indistinguishable cells did enter the structure (lower panel). Gray bars, *Edg1*$^{+/+}$ and white bars, *Edg1*$^{-/-}$ T cells. Calculations were performed for 2 intravital movies (IVM) (2 mice) with observation from the cortical side (C) and 2 movies of explanted lymph nodes (2 mice) with one imaged from the cortical and one from the medullary side (M). For each experiment n indicates tracked number of events when T cells leave outer border of sinus either into parenchyma or inside the sinus. **(d)** Distribution of time spent at the outer border of cortical LYVE-1$^+$ sinuses for *Edg1*$^{+/+}$ T cells (top panel) and *Edg1*$^{-/-}$ T cells (lower panel) combined from two intravital

experiments (2 mice). Light gray bar shows data for cells that contacted the sinus border and left within the tracking time; dark gray bar shows data for cells that arrived at the border before the tracking began or were still at the border at the end of the tracking. **(e)** Velocities of *Edg1*$^{+/+}$ and *Edg1*$^{-/-}$ T cells outside LYVE-1^{+} sinuses (light gray**)** (median velocities 16.1 and 14.0 μm/min) or at their borders (dark gray) (median velocities 16.2 and 14.5 μm/min). Data are from two intravital experiments (2 mice). **(f)** Relative propensity of *Edg1*$^{+/+}$ and *Edg1*$^{-/-}$ T cells to move towards LYVE-1^{+} sinuses. The ratio of *Edg1*$^{+/+}$ and *Edg1*$^{-/-}$ T cell transition frequency into the area within 0 −10, 10 − 20 and 20 − 30 μm away from the sinus, calculated for 2 intravital (black and gray circles) and 1 explant (white circles) movie (3 mice) was determined as detailed in Methods.

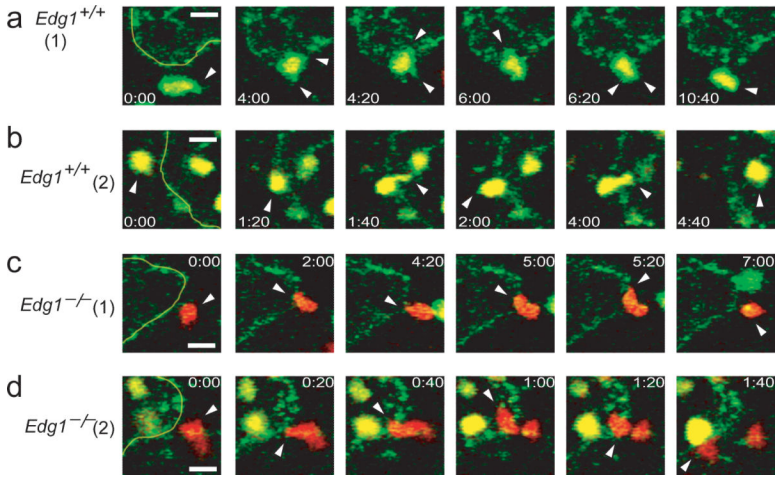

Figure 3. Wild-type and S1P$_1$-deficient T cells extend processes into LYVE-1$^+$ cortical sinuses during entry decision-making

a-d, Time-series images obtained by two-photon microscopy of explanted inguinal lymph node. *Edg1*$^{+/+}$ T cells double-labeled with CFSE and CMTMR (**a, b**) and *Edg1*$^{-/-}$ T cells labeled with CMTMR (**c, d**) are shown approaching LYVE-1$^+$ cortical sinuses, labeled with LYVE-1 specific antibody (green). White arrows indicate the location of cell processes. *z*-projections are from two *z* planes 3 μm apart (**a, c and d**), or a single z plane (**b**). Elapsed time is shown as mm:ss. Data in a-d are from two independent experiments (2 mice). Scale bar, 10 μm. See also Supplementary movie 3.

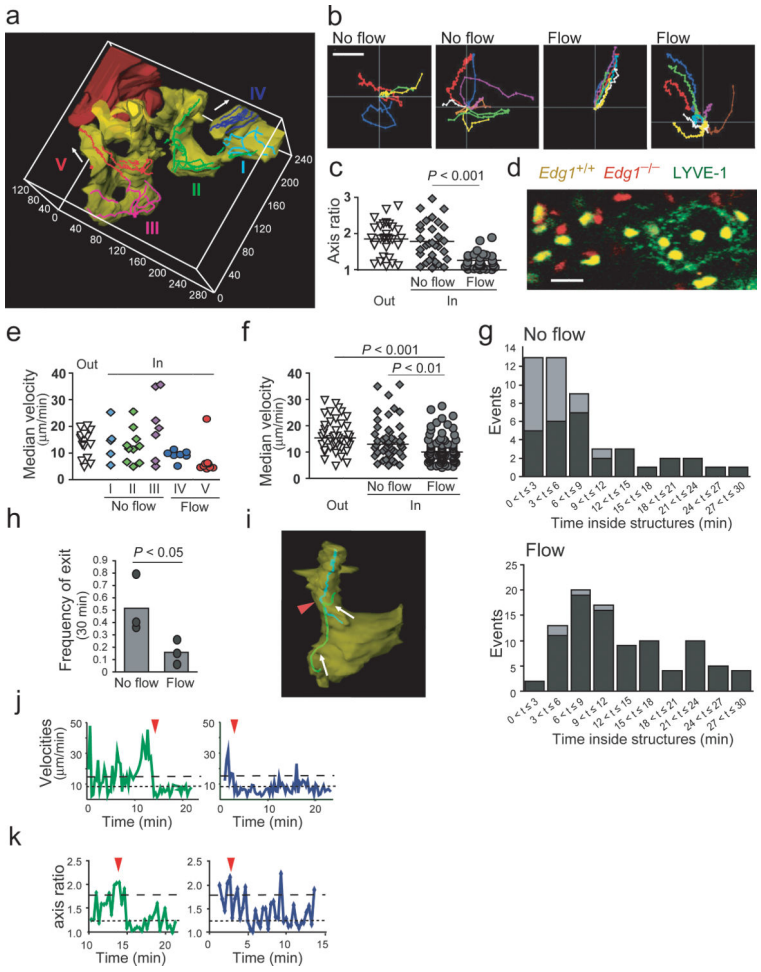

Figure 4. Directional flow and T cell retention inside LYVE-1$^+$ cortical sinuses

(a) Three-dimensional reconstruction of LYVE-1$^+$ structures imaged by two-photon intravital microsopy of inguinal LN. The structure was subdivided into macrophage-rich sinus area (red) and cortical sinuses (yellow) as described in the Methods. Colored tracks represent trajectories of *Edg1*$^{+/+}$ T cells inside various interconnected regions of LYVE-1$^+$ positive sinuses. See also Supplementary movie 5. **(b)** Superimposed tracks of cells in regions I, II (first 2 panels) and IV, V (last 2 panels) of **a**, in the *xy* plane, setting the starting coordinates to the origin. Scale bar, 30 μm. **(c)** Axis ratio of cells outside LYVE-1$^+$ cortical sinuses (white triangle), in the regions of the sinuses with random cell movement (gray diamond) and in the regions with directional cell movement (gray circle). Data are combined from two intravital experiments (2 mice) and medians are shown by horizontal lines. **(d)** Two-photon microscopy image of T cell morphology in the parenchyma and inside a LYVE-1$^+$ cortical sinus with directional cell movement. The image is a 6 μm *z* projection and the cells and structures were labeled as indicated. **(e)** Velocities of *Edg1*$^{+/+}$ T cells from experiment illustrated in **a**. Velocities are shown for cells outside LYVE-1$^+$ cortical sinuses (white triangles), and in sinus regions without flow (diamonds) and with flow (circles). Color-coding corresponds to the cortical sinus regions in **a**. **(f)** Velocities of *Edg1*$^{+/+}$ T cells from three intravital experiments (3 mice). Median velocities were calculated for each

period of time that cells spent outside sinuses (white triangles) or inside sinuses without flow (diamonds) and with flow (circles). **(g)** Distribution of time spent by *Edg1*$^{+/+}$ T cells inside cortical LYVE-1^{+} sinuses in regions without flow (top panel) and with flow (lower panel). Data are pooled from three intravital experiments (3 mice). Light gray bars indicate tracks that entered and left the sinus within the tracking time. Dark gray bars indicate cells that transmigrated inside before the tracking began or were still inside at the end of the tracking. **(h)** Fraction of cells inside LYVE-1^{+} cortical sinuses that returned to the parenchyma within 30 min of tracking in regions without flow and with flow. Data are from three intravital experiments (3 mice). Bars indicate means. **(i)** Trajectories of two T cells tracked in green and blue migrating within a LYVE-1^{+} cortical sinus from a region without flow into an adjacent region where they are “captured” by flow at the position indicated by the red arrow. Image shows a fragment of region II from **a**. **(j and k)** Changes in the apparent velocities and axis ratio of the T cells shown in **i**. Red arrow indicates the location where the green and blue tracks cross into the region of flow. Velocity data are shown for the entire track duration whereas cell shape index data are shown for part of each track as indicated, where time zero indicates the start of imaging. Dashed lines indicate the median for cells in the absence of flow (long dashes) and in the presence of flow (short dashes), from c and f. Data in a, b, e are from one experiment that is representative of three (3 mice) and i-k are from one experiment that is representative of two (2 mice).

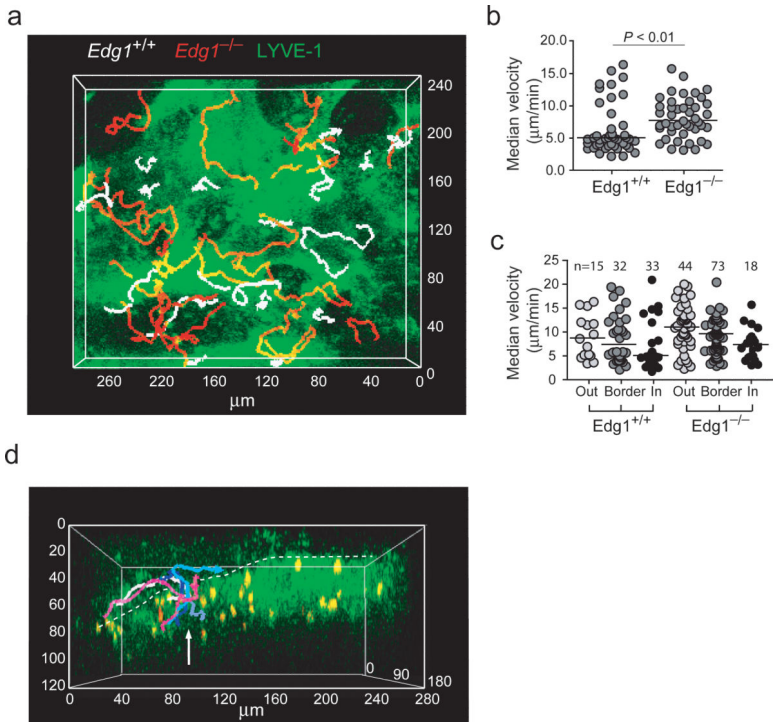

Figure 5. Comparison of *Edg1*$^{+/+}$ and *Edg1*$^{-/-}$ T cell behavior in the medullary region and *Edg1*$^{+/+}$ T cell exit into the subcapsular space

(a) Three-dimensional view of medullary LYVE-1^{+} structures (green) and trajectories of *Edg1*$^{+/+}$ (white tracks) and *Edg1*$^{-/-}$ (red tracks) T cells. See also Supplementary movie 7. **(b)** Median cell velocities of *Edg1*$^{+/+}$ and *Edg1*$^{-/-}$ T cells in the medullary region. Horizontal lines indicate medians. **(c)** *Edg1*$^{+/+}$ and *Edg1*$^{-/-}$ T cell velocities with respect to the LYVE-1^{+} medullary structures. Cell velocities were evaluated in the areas outside (light gray), on the border (dark gray) and inside (black) the LYVE-1^{+} structures. Horizontal lines indicate medians. n indicates number of events. Data in a are representative of three independent experiments and the tracking analysis in b and c was performed in one experiment. (**d)** Medullary side of the lymph node where T cells flow into the hilar region. Three-dimensional view of the LYVE-1^{+} structures (green) and *Edg1*$^{+/+}$ T cells (yellow). Dotted line outlines contour of the subcapsular space. The tracks are of cells that flow through the medullary sinus into the subcapsular region. White arrow indicates direction of movement. Data are representative of two intravital imaging experiments. See also Supplementary movie 8.